Vacancy-hydrogen interaction in H-implanted Si studied by positron annihilation

R. S. Brusa, M. Duarte Naia, and A. Zecca
Dipartimento di Fisica, Università di Trento, I-38050 Povo TN, Italy

C. Nobili, G. Ottaviani, and R. Tonini
Dipartimento di Fisica, Università di Modena, I-41100 Modena MO, Italy

A. Dupasquier
Dipartimento di Fisica, Politecnico di Milano, Piazza Leonardo da Vinci 32, I-20133 Milano MI, Italy
(Received 22 December 1992)

The density of vacancylike defects, produced in silicon by hydrogen implantation at 15.5 keV and surviving to successive isochronal annealings, has been measured by means of a slow positron beam. The results show that the number of defects acting as positron traps is a small fraction of the Frenkel pairs produced by implantation. This number decreases, increases again, and eventually disappears after annealing at increasing temperatures. The mean depth of the positron traps in as-implanted samples is smaller than the mean depth of vacancies predicted by computer simulations, but reaches, and in some cases surpasses, this limit after annealing. A minimum in the number of the positron traps occurs around 350 °C when the number of displaced silicon atoms, produced by hydrogen agglomeration, is at maximum. Further annealing increases the number of traps, until at high temperatures, above 700 °C, all the traps disappear. This complicated behavior is interpreted as the result of several concomitant effects: the formation of vacancylike defects during implantation, their partial annealing below 350 °C, an initial passivation of the traps caused by hydrogen followed by a reactivation stage, and the formation of thermally stable hydrogen complexes.

I. INTRODUCTION

Incorporation of hydrogen in crystalline silicon (*c*-Si) by ion implantation is a subject of scientific and technological relevance which has received intense attention for more than two decades (for orientation on this matter, see Refs. 1 and 2). Hydrogenation affects structural and electric properties of *c*-Si in a rather complex way, which depends in part on the implantation conditions (flux, fluence, energy, temperature), and in part on the thermal history of the sample. A crucial role in determining the final conditions of the material is played by the interaction of the implanted hydrogen with the defects created by implantation.

In the last few years, a systematic effort for studying the hydrogen-defect interaction in *c*-Si has been performed by a group of investigators, including some of the present authors.[3–6] The guiding idea behind this series of works was to reduce the complexity of the problem, by concentrating attention on silicon samples implanted at an energy (15.5 keV) low enough to avoid the production of dense collisional cascades. Several experimental techniques [secondary-ion-mass spectroscopy (SIMS), Rutherford backscattering (RBS) in channeling conditions, x-ray diffraction (XRD), infrared spectroscopy, elastic recoil detection analysis, transmission electron microscopy (TEM), and high-resolution electron microscopy (HREM)] have been used so far to characterize these samples with respect to different aspects: density profiles of total hydrogen and of the molecular form H_2, residual hydrogen content after thermal annealings, displacement field of Si, spectrographical identification of various bound states of hydrogen, and direct TEM and HREM detection of local disorder. The present work completes this series of experimental analysis by the measurement of the density profiles of vacancylike defects, as detected by positron annihilation.[7]

The use of positrons as defect probes for vacancylike defects is a well-established technique [positron-annihilation technique, (PAT)], whose physical bases have been known since the late 1960s (for general reviews, see Refs. 8 and 9). Only in recent years, however, has PAT been extended to the measurement of density profiles of subsurface defects, owing to technical progress in producing positron beams of variable energy (a recent review on positron beams is in Ref. 10). Specific examples of the use of positron beams for the study of damage produced by ion implantation in *c*-Si are in Refs. 11–13.

As in the examples cited above, and also in the present instance, the positron-beam method gives good results concerning the detection of vacancylike defects. Our data, however, bring out an aspect that did not emerge in such a clear way in any previous work. Let us briefly explain this point. Detection of vacancylike defects by positrons is made possible by the phenomenon of positron trapping, which occurs in open-volume regions of any kind of crystalline material. In dielectrics, however, positron trapping is strongly influenced by the charge state of the defect and by the presence of associated impurities, which may passivate the trap. In particular, the passivation effect of hydrogen on positron traps at the interface SiO_2/Si has been shown in Refs. 14–16. In the present

 ©1994 The American Physical Society

experimental situation, passivation is clearly demonstrated by the effects of thermal annealing on positron trapping. We thus have direct proof that the increased displacement field, observed by RBS after moderate annealing,[4] is related to hydrogen saturation of the vacancy complexes. It is another piece of a jigsaw puzzle that fits into the right place of an almost complete picture.

This paper is organized as follows. In Sec. II, we give the necessary information regarding sample preparation and treatments, as well as measurement procedures and setup. The experimental results are presented and briefly commented on in Sec. III. Our interpretation is discussed and some conclusions are drawn in Sec. IV. The details of the mathematical model adopted for reducing the raw data of positron measurement to defect density profiles, which are essential for reconstructing our analysis procedures, but are perhaps more interesting for the specialized public of positron physicists than for a general readership, are left to the Appendix.

II. EXPERIMENTAL PROCEDURES

We have examined three series of samples.

(a) Room temperature (RT)(p) series: single crystals of Czochralski p-type silicon (resistivity 16–24 Ω cm), obtained from 4-in.-diam slices, (100) oriented. Implantation was carried out at RT with H_2^+ (beam current density 1 mA/cm^2) impinging on the sample at an energy of 31 keV with an inclination of 7° from the normal to the exposed surface. Because of H_2 fragmentation at the surface, this is equivalent to implantation of atomic hydrogen at a double fluence [$(1.3-1.6)\times 10^{16}$ H/cm^2] and an energy of 15.5 keV. The temperature increase during implantation was below 100 °C. After implantation, different thermal treatments were performed for the various samples of the series, by heating in a vacuum for 2 h at one of the following temperatures: 350, 500, 700, 800, and 900 °C.

(b) Liquid-nitrogen temperature (LNT)(p) series: implantation carried out at LNT, with a beam current density of 1 μA/cm^2, up to a fluence of 1.6×10^{16} H/cm^2. Any other details are the same as above.

(c) LNT(n) series: single crystals of Czochralski n-type silicon (resistivity 7–10.5 Ω cm). The maximum anneal temperature is 500 °C (at this temperature, most of the important effects discussed below are already observable; samples annealed at higher temperatures were not available). Any other details are the same as for the LNT(p) series.

The positron-annihilation measurements were carried out using a variable-energy beam, supplemented by a 74 MB$_q$ β^+ source of Na.[22] In this setup, the fast positrons coming from the β^+ source are moderated passing through a 4-μm tungsten foil, accelerated to 200 eV, transported at constant energy by a bent solenoid, and reaccelerated at the end of the trajectory by giving a negative bias to the sample (from 0.2 to 30 keV).

The detection of positron trapping by defects was performed by the so-called Doppler-broadening method, which is based on the sensitivity of the shape of the 511 keV annihilation line to the momentum distribution of the electrons giving annihilation.[17] We used a high-purity Ge spectrometer (energy resolution of 1.8 keV at 1.33 MeV), with software stabilization. The data were collected according to the "microspectrum method."[18] The shape of the annihilation line was characterized by means of the usual S parameter (fractional area of the line in a fixed energy window centered at a 511-keV peak). The S parameter is always larger for positrons annihilated in vacancylike defects than for positrons annihilated in the ordered bulk. On the contrary, the characteristic value of S, for positrons annihilating at the surface of a sample, depends very much on the conditions of the surface, and can be larger or smaller than the bulk value S_b; for oxidized surfaces of c-Si, the surface value of S is normally below S_b.

III. RESULTS

The presence of vacancylike defects, acting as positron traps, is clearly visible through its effect on the dependence of the S parameter vs the positron-beam energy E. Figure 1 compares, as an example, two curves of the RT series, referring to a virgin (nonimplanted) sample (curve a), and to a sample annealed at 350 °C after H implantation (curve b). The two curves may be qualitatively read as follows. The common high-energy asymptote represents the characteristic value for undamaged bulk material (S_b), and indicates that above ~15 keV, the positrons are implanted deep enough to annihilate beyond the disordered layer produced by implantation. At the $E=0$ extreme of the curves, the S parameter approaches the surface value S_s, which is slightly different for the two samples. This difference is not important in the present context, as it merely reflects different surface conditions of the two samples. The important differences are in the shape of the curves. Curve a runs monotonically between the extremes S_b and S_s, because the fraction of positrons diffusing back to the entrance surface decreases progressively with the increase of the implantation energy. On the contrary, a maximum appears

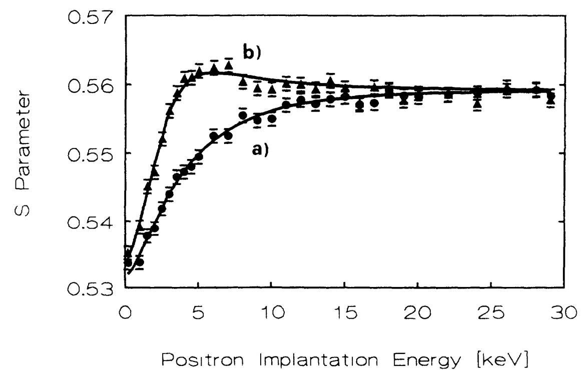

FIG. 1. An example of the effect of positron trapping on the shape parameter S; the horizontal axis gives the positron implantation energy; the points on curve a are obtained for virgin p-type c-Si and those on curve b are for the same material, after RT hydrogen implantation and annealing at 350 °C. The best-fit curves are from the diffusion model.

around 4 keV in curve *b*; this shows that the positrons implanted with this energy come to rest in a region where there is an important concentration of positron traps, thus forming a localized state characterized by a shape parameter S_d well above S_b and S_s.

The effect of positron trapping can be shown with greater evidence by reelaborating the *S* data in terms of the difference

$$\Delta = \frac{S - S_s}{S_d - S_b} - \frac{S_b - S_s}{S_d - S_b}\left[\frac{S - S_s}{S_b - S_s}\right]_{\text{virgin}} , \qquad (1)$$

where the subscript virgin refers to a nonimplanted reference sample. In the calculation of the above expression, we have used the same values $S_b = 0.5592$ and $S_d = 1.037 S_b$ for all samples, and assigned to S_s a value individually determined for each sample. The choice of the above values is discussed in the Appendix.

Our experimental results are presented in terms of Δ in Figs. 2–4, respectively, for the RT(*p*), and LNT(*p*), and the LNT(*n*) series. In these figures, the upper horizontal axis gives the (nonlinear) scale of average positron-implantation depths, calculated as discussed in the Appendix; it can be useful for assessing, at first sight, the depth from which the trapping signal is coming.

The data shown in Figs. 2–4 contain the physical in-

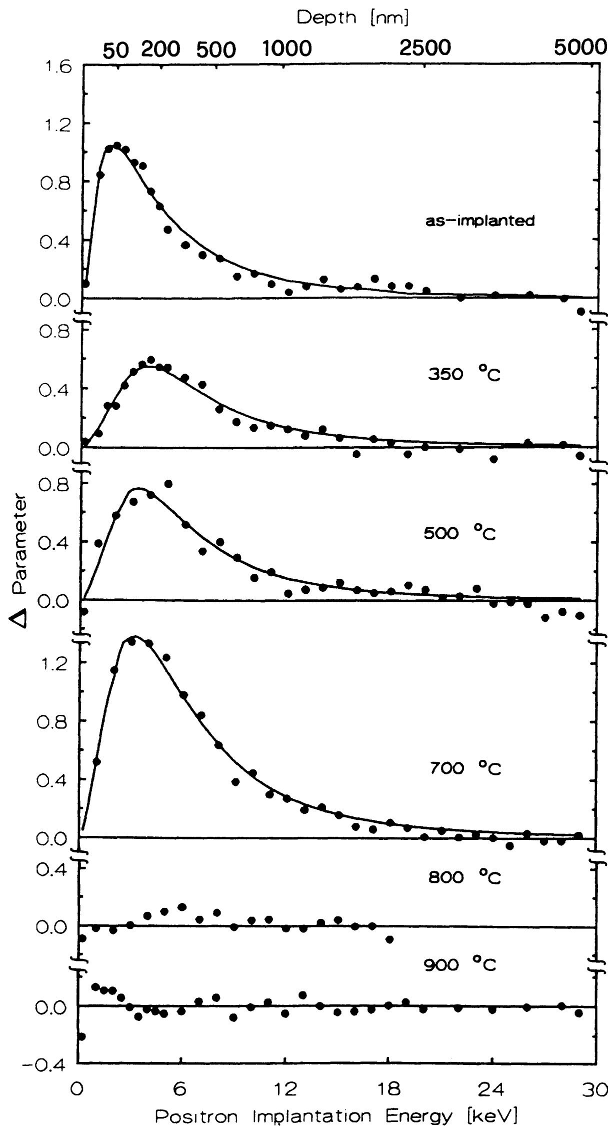

FIG. 2. Parameter Δ plotted vs positron implantation energy *E* [RT(*p*) series]; the upper horizontal axis gives the mean implantation depth of the positrons. Best-fit curves from the diffusion model.

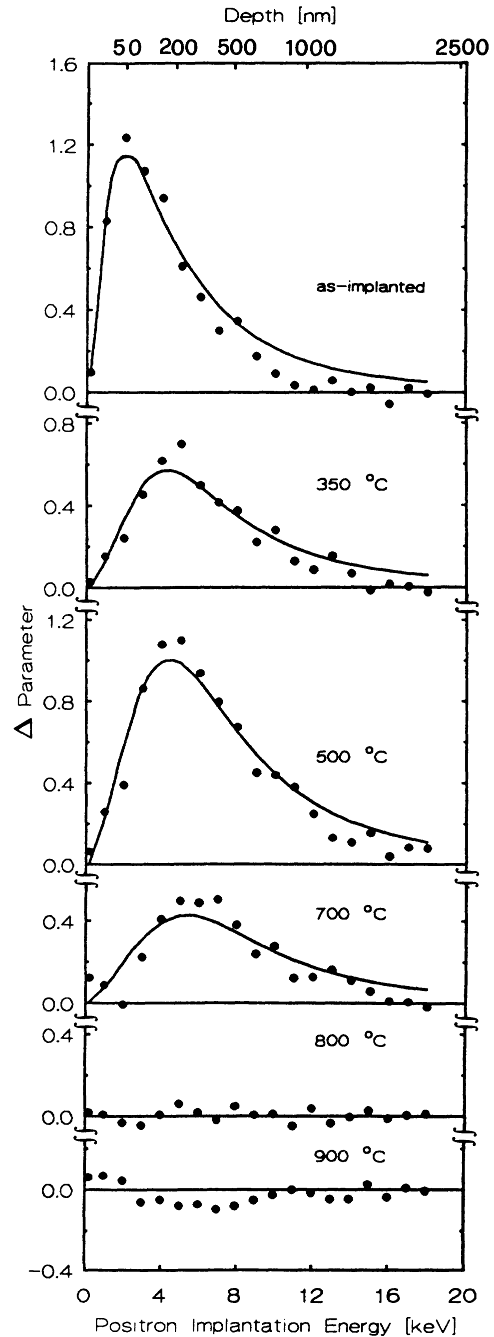

FIG. 3. Parameter Δ plotted vs positron implantation energy *E* [LNT(*p*) series]; the upper horizontal axis gives the mean implantation depth of the positrons. Best-fit curves from the diffusion model.

formation needed for the mathematical reconstruction of the defect density profiles discussed below. However, we want to draw the attention of our reader to the points that emerge from these figures at the first visual inspection. (a) The defect signal is strong in the as-implanted samples, decreases with annealing at 350 °C, increases again with annealing at 500 °C, and drops to zero only with annealings at 800 °C. (b) Annealing at 350 °C and above increases the depth from which the signal comes.

Let us now proceed to the results of the quantitative analysis, based on the diffusion model discussed in the Appendix. In this analysis, the shape of the defect density profile has been assigned on the basis of a guess guided by a computer simulation; the integral and the mean depth of the profile were left as free parameters to be adjusted by the best-fit procedure. The outcome is presented in Table I: here, $\bar{d}$ is the mean depth of the defect distribution, and N^* is a parameter proportional to the integral of this distribution, which physically represents the total number N of defects per unit area of the sample. N and N^* are related by the equation

$$N^* = \frac{\nu}{\nu_{1v}} N \; , \qquad (2)$$

where ν is the positron specific-trapping rate of the defects, and $\nu_{1v} = 1 \times 10^{14}$ s^{-1} is the nominal specific-trapping rate for neutral monovacancies.[19] Without information on the defect species acting as positron traps present in the material at various stages of annealing (we shall discuss this point below), it is impossible to convert N^* in the actual defect number N. However, according to the crudest approximation, which assumes that the positron specific-trapping rate for a cluster of n vacancies is proportional to n, one could use Eq. (2) with the simplification $\nu/\nu_{1v} = n$. In the spirit of this approximation, N^* would represent the total number of monovacancies needed to form the actual trap population. We shall thus consider N^* as an "effective vacancy number," although isolated monovacancies are thought not to be stable in Si at room temperature. (However, see Ref. 20.)

TABLE I. Results of the analysis of the S vs E curves, according to the diffusion model: N^* is the effective number of vacancies per unit surface and $\bar{d}$ is the mean depth of the defect density profile.

Sample	N^* (10^{15} cm^{-2})	$\bar{d}$ (nm)
RT(p) series:		
As implanted	1.0±0.15	19±3
Ann. 350 °C	0.2±0.03	146±20
Ann. 500 °C	0.4±0.05	96±20
Ann. 700 °C	3.3±0.40	118±30
Ann. 800 °C	Not detected	
Ann. 900 °C	Not detected	
LNT(p) series:		
As implanted	1.1±0.15	24±5
Ann. 350 °C	0.1±0.03	180±30
Ann. 500 °C	0.4±0.05	210±30
Ann. 700 °C	0.1±0.03	320±30
Ann. 800 °C	Not detected	
Ann. 900 °C	Not detected	
LNT(n) series:		
As implanted	0.7±0.10	42±5
Ann. 350 °C	0.3±0.05	158±20
Ann. 500 °C	0.8±0.12	202±20

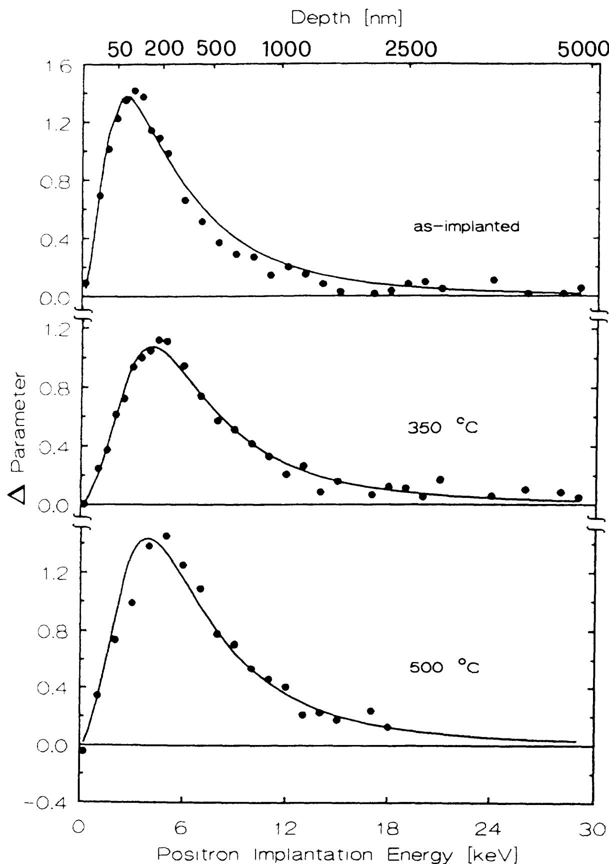

FIG. 4. Parameter Δ plotted vs positron implantation energy E [LNT(n) series]; the upper horizontal axis gives the mean implantation depth of the positrons. Best-fit curves from the diffusion model.

The experimental indeterminations reported in Table I reflect the statistical uncertainty of the best-fit analysis, which was taken equal to the interval, where the increase of the variance of the fit [χ^2/n_d, where n_d is the number of degrees of freedom] above its minimum remains below $1/\sqrt{n_d}$. Systematic errors are discussed in the Appendix.

The data in Table I not only confirm in quantitative terms the findings cited above as points (a) and (b), but also enable us to note the following. (c) The effective number of positron traps in as-implanted samples $\sim 1 \times 10^{15}$ cm^{-2} is a fraction of the Frenkel pairs that survives recombination and out diffusion during the implantation and the room-temperature aging of the samples (from RBS measurements, one observes about 2.5 surviving self-interstitials per implanted ion.[4] Therefore, one would expect a total of 4×10^{16} cm^{-2} not recombined Frenkel pairs for the RT series and for the LNT series.

(d) In the as-implanted samples, the mean depth of the positron-trap profile (from 19 to 42 nm) is much shallower than the value predicted ($\bar{d}=130$ nm) on the basis of a computer simulation by the MARLOWE code.[21]

Figure 5 (upper part) gives some examples of density profiles of positron traps, as obtained from the best-fit analysis of the S vs E data data and the density profile of vacancies calculated by molecular-dynamic simulation (MARLOWE code).[21] The lower part of the figure also shows, for comparison, the density profile of hydrogen obtained from SIMS, and an indication on the localization of extended defects revealed by TEM cross sections. The figure refers to the RT(p) series. The comparison of the curves clearly shows that annealing increases the mean depth of the positron traps, and moves the hydrogen peak to shallower depth. Note that SIMS curves are cut at densities below 10^{19} at./cm^3, which corresponds to the sensitivity limit in the operating conditions of this experiment.

In view of the discussion presented in Sec. IV, we recall here some important elements emerging from experiments by complementary techniques.

RBS analysis is unable to detect single vacancies and small vacancy clusters. However, RBS reveals, in the region from the surface down to 160 nm, the presence of silicon interstitials, which is consistent with the presence

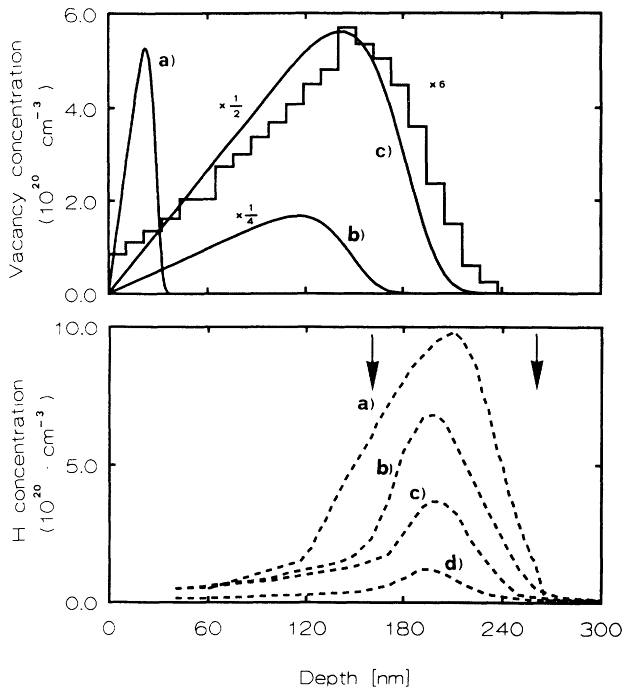

FIG. 5. Upper—vacancies concentration from PAT: (a) RT(p), as implanted; (b) RT(p), annealed 500 °C; (c) RT(p), annealed 700 °C. The bar diagram is the result of the molecular-dynamics simulation (Ref. 5) for the as-implanted sample. Lower—hydrogen concentration from SIMS (Ref. 6): (a) RT(p), as implanted; (b) RT(p), annealed 400 °C; (c) RT(p), annealed 450 °C; (d) RT(p), annealed 500 °C. The arrows mark the limits of the region where an average concentration of about 3×10^{21} extended defects/cm^3 has been observed with TEM in the as-implanted sample.

of vacancies observed by PAT in this region.

TEM analyses reveal an important concentration of extended traps in regions deeper than 160 nm, which do not seem to contribute substantially to positron trapping. Some examples of TEM cross sections are shown in Fig. 6. Figure 6(a) refers to an as-implanted sample of the RT series; it shows a damaged region extending from 160 to 260 nm. Most of the defects are {100} and {111} platelets, which are generally attributed to the presence of hydrogen. A few {113} platelets are due to the implantation process.[22] At 400 °C, Fig. 6(b), the platelets tend to increase in size (from 7 nm in the as-implanted sample up to 120 nm). The platelets caused by the hydrogen tend to disappear after 600 °C anneal [Fig. 6(c)]. At this temperature, three-dimensional defects, which are clearly identified at 700 °C, begin to appear. These defects show a lower electro-optical density suggesting the presence of hydrogen. Annealing at 800 °C produces the coalescence of the three-dimensional defects. The pictures in Fig. 6 were taken so as to evidence the defect structure. Consequently, the surface is not shown. For LN-implanted samples, the defect structure and thermal evolution are similar to the RT(p) series.

SIMS profiles of hydrogen concentration, shown in Fig. 5, are peaked in the region containing extended defects. Actually, the combination of SIMS, RBS, and XRD analyses[4] shows that two kinds of hydrogen complexes are present in heavily implanted samples; one type, which disappears around 200 °C, is bound to point defects; a second type, much more stable, is present in the sample even after the 700 °C anneal. The latter complex is responsible for a large displacement field in the silicon lattice. The maximal displacement field occurs around 350–400 °C, i.e., in the same temperature interval where the positron-trap density is minimum.

Preliminary deep-level transient spectroscopy (DLTS) measurements on samples of the RT(p) series have revealed the presence of the hole traps at 0.67 and 0.33 eV from the edge of the valence band. It is interesting to note that the concentration of these traps, which are most probably to be identified with vacancy-hydrogen complexes, follows a pattern very similar to that observed for positron traps: it decreases with the annealing at 350 °C, increases at 500 °C, and disappears at 800 °C.

IV. DISCUSSION

The number of vacancies detected by PAT is small in comparison with the number of self-interstitials estimated from RBS data. This result may, in part, be explained by the larger probability of out-diffusion of vacancies in comparison to self-interstitials. However, it seems more likely that the observed effect is due to the association of vacancylike defects with hydrogen (most probably H^+), that leads to their passivation as positron traps.

Even more complex is the situation for the annealed samples, where the number of traps decreases, increases, and finally goes to zero with increasing annealing temperature. We interpret the evolution of the positron-trapping signal according to the following steps.

(a) In as-implanted samples, a small number of active

(a)

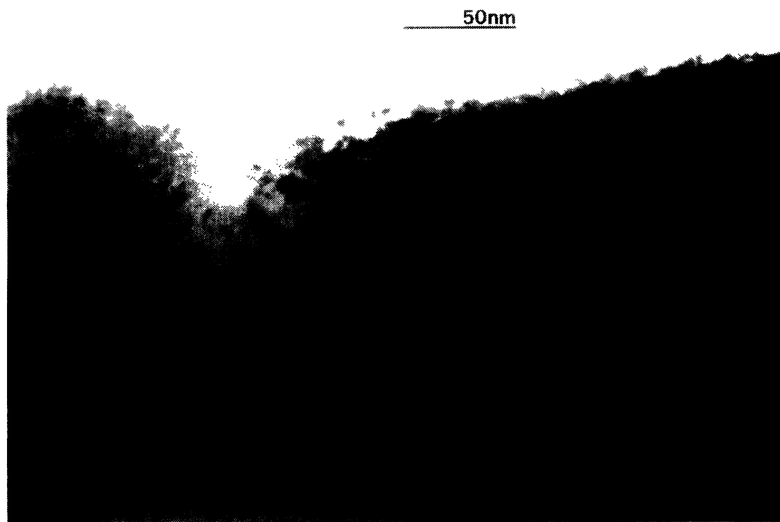

(b)

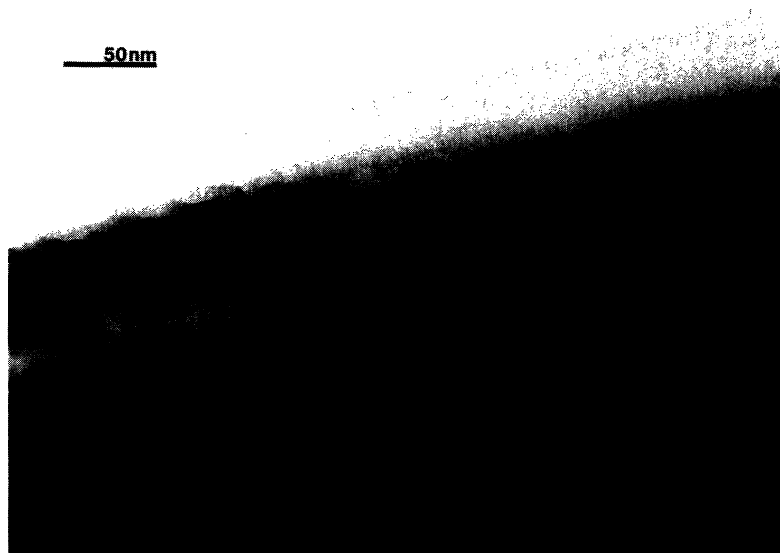

(c)

FIG. 6. TEM cross section of three RT(p) samples: (a) as-implanted; (b) annealed at 400 °C; (c) annealed at 600 °C.

positron traps (probably small vacancy clusters) survives at a shallow depth, where hydrogen is practically absent; other potential positron traps exist at larger depths, but are mostly passivated by the weakly bound H.

(b) Annealing at 350 °C has the effect of removing divacancy, three-, and four-vacancy clusters, which are all mobile above $\sim$330 °C.[1,23] Residual implantation defects not decorated by hydrogen give the weak positron-trapping signal observed after the first annealing stage; all the hydrogen associated to extended defects remain in place.

(c) SIMS measurements tell us that at 500 °C only about 10% of the initial concentration of H is still present.[6] Thus, some of the previously passivated positron traps, existing around and above 100 nm, become active, and originate the increase in the trapping signal at 100–150 nm observed with the anneal at 500 °C.

(d) Positron trapping conditions after annealing at 700 °C are the results of two competing factors: the passivation effect of hydrogen is now strongly reduced, but, on the other hand, the number of surviving traps decreases since also large vacancy clusters tend to disappear. The first of the two effects prevails in RT samples, the second in LNT samples, where vacancy clusters tend to be smaller due to the reduced motion of vacancies during irradiation.

(e) Annealing at and above 800 °C eliminates any positron trap.

In conclusion, we have observed the evolution of the vacancy-hydrogen association at various stages of thermal annealing of H-implanted *c*-Si. Our observations are perfectly consistent with the complementary RBS evidence concerning the evolution of the Si displacement field.[4] Taken together, the two experiments tell us that the escape of hydrogen from vacancy clusters, observed by PAT, leads to the formation of supermolecular hydrogen complexes, which is the primary cause of the increase of the displacement field revealed by RBS.

We have also obtained clear proof of the passivation of positron traps due to hydrogen. This effect has been mentioned before.[12,14–16] In particular, the results of Ref. 12 show many points of similarity with ours. In particular, one notes the increase of the average depth of the positron traps after the first stages of annealing, which, in our interpretation, is not related to the motion of the vacancies but to the reactivation of deep traps that were passivated by hydrogen trapping. The main difference between the present work and Ref. 12 is the effectiveness of the passivation, which is almost total in our case and only partial in the other experiment. We see the reason for this difference in the higher energy of H implantation (35–100 keV) in Ref. 12, which leaves an extended region where point defects do not overlap with hydrogen.

Another interesting point, on which our observations again converge with those of Refs. 11–13, is the persistence of positron traps up to 700 °C. We have seen, at least in one case (the RT series), that this can be a surprisingly large effect. The easiest, and probably true, explanation is the existence of vacancy clusters formed by five or more units, whose formation in the RT series has been favored by the higher mobility of defects during irradiation. A nonsecondary role could have been played, however, by the stabilization of vacancy clusters due to the association with hydrogen. A hint in this direction is the greater depth of the positron-trapping signal in the LNT series after annealing, which indicates stable defects surviving beyond the maximum of the Frenkel pair concentration by the computer simulation, i.e., displaced toward the maximum of the hydrogen concentration. We think that this subject deserves further investigation.

By testing samples of different carrier sign, but implanted in the same direction [the LNT(p) and the LNT(n) series], we have specifically tried to reveal charge-state effects, that are sometimes extremely evident in *c*-Si.[24,25] In fact, no large differences seem to exist between these LNT(p) and LNT(n) series. Most probably, the Fermi-level position in the damaged region is independent on the doping of the material, and, therefore, the charge state of the potential positron traps is almost the same in the two series of samples. Still, doping affects the positron distribution through the internal fields associated with local band bendings. We have done our best to take accurately into account the effect of near-surface fields (see the Appendix). Nevertheless, we believe that internal fields are a factor influencing negatively the accuracy of depth evaluations from PAT data.

APPENDIX: ANALYSIS OF PAT DATA

The determination of the parameters characterizing the positron-trap profile ($N^*,\bar{d}$) is based on the best fit of S vs E data. The model adopted (diffusion model) derives from the following widely accepted assumptions.

(a) The measured S parameter is the linear combination of three energy-independent terms S_b, S_s, and S_d, as given by the equation

$$S = p_b S_b + p_s S_s + p_d S_d \ , \tag{A1}$$

where the coefficients of the linear combination (p_b, p_s, p_d) are the probabilities of annihilation, respectively, in the bulk, at the surface, or in a defect.

(b) The coefficients p_b, p_s, p_d depend on the implantation energy; they are related to the stochastic stationary density of thermal positrons at depth z by the equations

$$p_b = \lambda \int_0^\infty n(z)dz , \tag{A2}$$

$$p_s = D_+ \left[\frac{dn}{dz} \right]_{z=0} , \tag{A3}$$

$$p_d = \nu \int_0^\infty C(z) n(z) dz \ , \tag{A4}$$

where λ is the bulk annihilation rate for *c*-Si [for which we have taken the experimental value $(220\ \mathrm{ps})^{-1}$ (Ref. 26)], D_+ is the positron diffusion constant (the assignment of the numerical value of this parameter is discussed below), ν is the specific trapping rate per unit defect concentration, and $C(z)$ is the concentration of positron traps.

(c) The positron density n is the solution of the one-dimensional drift-diffusion equation:

$$D_+ \frac{d^2 n}{dz^2} - \frac{d}{dz}(\mu_+ \mathcal{E}_z n) - [\lambda + \nu C(z)] n + P(z) = 0 \ , \tag{A5}$$

where μ_+ is the positron mobility, related to the diffusion constant and to the thermal energy k_BT by the Einstein equation $\mu_+=eD_+/(k_BT)$, $\mathcal{E}_z$ is the local electric-field component in the direction of the z axis, and $P(z)$ is the positron density at the end of thermalization (henceforth, called "positron implantation profile." The boundary conditions $n(0)=n(\infty)=0$ and the normalization condition for the implantation profile

$$\int_0^\infty P(z)dz=1 \qquad \text{(A6)}$$

automatically ensure the normalization of the probabilities:

$$p_b+p_s+p_d=1 \ . \qquad \text{(A7)}$$

Equation (A1) enables us to calculate the numerical value of S for each value of the implantation energy, when the parameters S_d,S_d,S_b are fixed, and p_s,p_d,p_b are calculated from the solution to Eq. (A5).

In the present analysis, S_b and S_d were kept fixed at the same values for all samples. For S_b, we have taken the average (0.5592) of all S data measured for beam energies above 20 keV, which are coincident within their error bars; modifications of the assumed value within the limits of its statistical accuracy (±0.0001) do not affect the final results of our analysis in a significant way. For S_d, we have taken the value $1.037S_b$, which was obtained by fitting S data for the sample which gives the highest trapping signal; we recall, for comparison, that Keinonen *et al.*[12] suggest the very similar relationship $S_d=1.034S_b$. It is to be mentioned that the choice of S_d strongly affects the determination of N^* when the local density of positron traps is so high that the peak experimental value of S is close to the saturation value S_d. In the present case, this situation occurs for the sample RT(p), 700 °C; here, decreasing S_d to the low limit of the best-fit indetermination ($S_d=1.031S_b$) leads to a 90% increase of N^*; in all other cases, the increase is below 30%. The values of S_s have been treated as best-fit parameters, in order to take into account the variability of the surface conditions of our samples. The range of values obtained for S_s is extended from $0.919S_b$ to $0.969S_b$.

The solution of Eq.(A5) was obtained by means of a computer routine[27] accepting any analytical or numerical form for the functions $P(z)$, $\mathcal{E}_z(z)$, and $C(z)$. Here we must explain our choices regarding these functions.

Positron implantation profile $P(z)$

A well-known approximation for the positron implantation profile is the Makhov function suggested by Valkealathi and Nieminen:[28]

$$P(z)=\frac{m}{z_0}\left[\frac{z}{z_0}\right]^{(m-1)}\exp\left[-\left[\frac{z}{z_0}\right]^m\right] , \qquad \text{(A8)}$$

where $M=1.9$ and z_0 is a depth parameter related to the mean implantation depth $\bar{z}$ by the equation

$$z_0=\bar{z}/\Gamma[(1/m)+1] ; \qquad \text{(A9)}$$

in turn, $\bar{z}$ depends on the implantation energy and on the density of the material ρ according to the equation

$$\bar{z}=\frac{\alpha}{\rho}\left[\frac{E}{1\ \text{keV}}\right]^n , \qquad \text{(A10)}$$

with the empirical values $\alpha=4\times10^{-6}$ g/cm^2 and $n=1.6$.

However, the Valkaelathi-Nieminen approximation is acceptable in the experimental conditions of our work at positron energies sufficiently large (a few keV) for avoiding that some positrons escape from the sample through the entrance surface before having completed their thermalization. Due to the negative bias of the sample, in our experimental setup these positrons are returned onto the sample and contribute to the implantation profile with a component different from zero at the surface. Therefore, we have adopted the Valkealathi-Nieminen approximation only for energies above 2.5 keV. Below this limit we have taken, instead, the modified profile

$$P(z)=\frac{1}{1.3862}\frac{1}{z_0}\left[1+\frac{z}{z_0}\right]\exp\left[-\left[\frac{z}{z_0}\right]^2\right] , \qquad \text{(A11)}$$

with

$$z_0=\bar{z}/0.6803 \ . \qquad \text{(A12)}$$

The dependence of $\bar{z}$ on E is still given by Eq. (A9), with $\alpha=3.7\times10^{-6}$ g/cm^2 and $n=1.7$, as determined in a previous experiment on Kapton.[29]

The depth scale reported in the upper horizontal axis of Figs. 2–4 is calculated by using Eq. (A10) with the different sets of α and n; the boundary between the two approximations ($E=2.5$ keV) was fixed at the point where the two scales match.

We have checked that extending the Valkaelathi-Nieminen approximation below 2.5 keV worsens the variance of the fit χ^2/n_d by about 10% without affecting $\bar{d}$ and N^*.

Electric field $\mathcal{E}_z$

The effect of near-surface fields on the positron distribution in the experimental conditions of this experiment is evident in our results for virgin samples of different carrier sign, shown in Fig. 7 in terms of the normalized shape parameter $(S-S_s)/(S_b-S_s)$. The shape of the curves in Fig. 7 indicates that the probability to reach the surface for a positron implanted at a given depth is larger in n-type samples than in p-type samples. In principle, two possible explanations of this different behavior could be proposed: (a) the positron diffusion coefficient is larger in n-doped than in p-doped silicon; (b) electric fields associated with band bending in the proximity of the surface attract the positrons toward the surface in n samples and push them away from the surface in p samples. The first hypothesis leads to an acceptable fit of the data, with a diffusion coefficient equal to 3.1 ± 0.1 cm^2/s for n-type silicon and to 2.2 ± 0.1 for p-type silicon; we do not see, however, any reasonable physical explanation for this marked difference of the diffusion coefficients, considering that the positron motion in materials with a modest

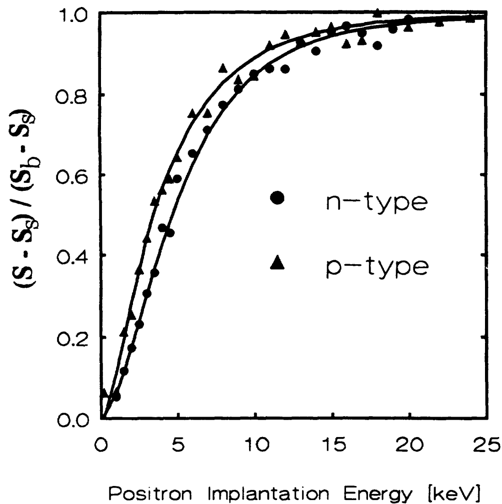

FIG. 7. Normalized shape parameter vs positron implantation energy for virgin c-Si: p type (triangles) and n type (full circles). Best-fit curves from the diffusion model.

impurity content should be limited, at room temperature, essentially by acoustical phonon scattering. We have thus taken into consideration the second hypothesis. Common wisdom regarding surface states indicates that, in most situations, the Fermi level at the surface is pinned by localized states at about one-third of the gap above the edge of the valence band. With this assumption, one predicts an electric field of the correct sign needed for explaining the differences shown in Fig. 7. However, the numerical fit of the experimental data turns out to be poor in the case of n-type samples. Therefore, we have left the surface-bulk potential differences V_n, V_p, and the diffusion coefficient D_+ as free parameters to be determined by best fit with the data for virgin samples, with the constraint that D_+ be the same for n and p samples. The electric fields associated with the assigned potentials were taken with the linear dependence on z predicted by the Poisson equation in the constant-carrier-density approximation. In accordance with estimates given in Ref. 27, the additional electric field due to the image force effect was neglected. The best fit was obtained for $D_+ = 3.1$ cm^2/s, $V_n = 0$ V, and $V_p = 69$ mV; the corresponding curves are reported in Fig. 7. The values obtained for virgin samples have been used for the analysis of the entire series of implanted and annealed samples.

Neglecting the electric field would considerably affect(30–40 %) the depths reported in Table I for the p-type series, and, in general, would worsen the fit.

Defect density profile $C(z)$

Determining the defect concentration $C(z)$ is the objective of our analysis. The most efficient use of the information contained in S vs E curves requires a reasonable guess on the functional form of $C(z)$, with a reduced number of best-fit parameters.

We have thus written $C(z)$ in the form

$$C(z) = \frac{\nu_{1v}}{\nu} \frac{N^*}{N_{\mathrm{Si}}} y(z) , \tag{A13}$$

where N_{Si} is the number of silicon atoms per unit volume, and $y(z)$ is the function describing the guessed form of the defect profile.

In order to check the sensitivity of the final results to the choice made for $y(z)$, we have tested two alternatives: (a) an analytical approximation of the shape of the vacancy profile predicted by the MARLOWE code (see bar diagram in Fig. 5),

$$y_1(z) = \frac{0.9329}{\bar{d}} \frac{z}{\bar{d}} \exp\left[- \left[\frac{0.6524 z}{\bar{d}} \right]^9 \right] , \tag{A14}$$

and (b) a smoother profile, with the shape of the derivative of a Gaussian,

$$y_2(z) = \frac{1.5735}{\bar{d}} \frac{z}{\bar{d}} \exp\left[- \left[\frac{0.887 z}{\bar{d}} \right]^2 \right] . \tag{A15}$$

The numerical constants in Eqs. (A14) and (A15) ensure the conditions

$$\int_0^\infty y_1(z) dz = \int_0^\infty y_2(z) dz = 1 , \tag{A16}$$

$$\int_0^\infty z y_1(z) dz = \int_0^\infty z y_2 dz = \bar{d} . \tag{A17}$$

The effective number of vacancies N^* and the mean depth $\bar{d}$ are adjustable parameters according to the best-fit criterion. The sensitivity of the final results to the alternative $y_1(z)$ or $y_2(z)$ is of the order of 5% for $\bar{d}$ and 15% for N^*. The values reported in Table I are the average of the two sets of results. The best-fit curves shown in Figs. 1–5 are obtained with the choice $y(z) = y_1(z)$.

[1] J. W. Corbett, J. K. Karins, and T. Y. Tan, Nucl. Instrum. Methods **182&183**, 457 (1981).

[2] S. J. Pearton, J. W. Corbett, and T. S. Shi, Appl. Phys. A **43**, 153 (1987).

[3] L. Meda, G. F. Cerofolini, R. Dierckx, G. Mercurio, M. Servidori, F. Cembali, M. Anderle, R. Canteri, C. Claes, and J. Vanhellemont, Nucl. Instrum. Methods B **39**, 26 (1989).

[4] G. F. Cerofolini, L. Meda, C. Volpones, G. Ottaviani, J. De Fayette, R. Dierckx, D. Donelli, M. Orlandini, M. Anderle, R. Canteri, C. Claeys, and J. Vanhellemont, Phys. Rev. B **41**, 12 607 (1990).

[5] L. Meda, G. F. Cerofolini, G. Ottaviani, R. Tonini, F. Corni, R. Balboni, M. Anderle, R. Canteri, and R. Dierckx, Physica B **170**, 259 (1991).

[6] L. Meda, G. F. Cerofolini, C. Bresolin, R. Diercks, D. Donelli, M. Orlandini, M. Anderle, R. Canteri, G. Ottaviani, R. Tonini, C. Claeys, J. Vanhellemont, S. Pizzini, and S. Farina, in *Proceedings of the Sixth International Symposium on Silicon Material Science and Technology*, edited by H. R. Huff (Sematech, Austin, TX, 1990), Vol. 90/7, p. 456.

[7] A very preliminary report of this experiment is in R. S. Brusa, M. Duarte Naia, A. Dupasquier, G. Ottaviani, R. Tonini, and

A. Zecca, Mater. Sci. Forum **105-110**, 1367 (1992).
[8] *Positron in Solids,* edited by P. Hautojärvi (Springer, Heidelberg, 1979).
[9] *Positron Solid-State Physics,* edited by W. Brandt and A. Dupasquier (North-Holland, Amsterdam, 1983).
[10] P. J. Schultz and K. G. Lynn, Rev. Mod. Phys. **60**, 701 (1988).
[11] J. Keinonen, M. Hautala, E. Rauhala, M. Erola, J. Lahtinen, H. Huomo, A. Vehanen, and P. Hautojärvi, Phys. Rev. B **36**, 1344 (1987).
[12] J. Keinonen, M. Hautala, E. Rauhala, V. Karttunen, A. Kuronen, J. Räisänen, J. Lahtinen, A. Vehanen, E. Punkka, and P. Hautojärvi, Phys. Rev. B **37**, 8269 (1988).
[13] P. J. Simpson, M. Vos, I. V. Michell, C. Wu, and P. J. Schultz, Phys. Rev. B **44**, 12 180 (1991).
[14] B. Nielsen, K. G. Lynn, Y. C. Chen, and D. O. Welch, Appl. Phys. Lett. **51**, 1022 (1987).
[15] P. Asoka-Kumar, K. G. Lynn, T. C. Leung, B. Nielsen, and X. Y. Wu, J. Appl. Phys. **69**, 6603 (1991).
[16] P. Asoka-Kumar, K. G. Lynn, T. C. Leung, B. Nielsen, Z. A. Weinberg, and G. W. Rubloff, Phys. Rev. B **44**, 5885 (1991).
[17] See, for instance, I. K. McKenzie in Ref. 9, p. 196.
[18] R. S. Brusa, M. Duarte, R. Grisenti, and A. Zecca, Mater. Sci. Forum **105-110**, 1853 (1992).
[19] S. Dannefaer, G. W. Dean, D. P. Kerr, and B. G. Hogg, Phys. Rev. B **14**, 2709 (1976).
[20] G. F. Cerofolini and L. Meda, *Physical Chemistry of, in and on Silicon* (Springer-Verlag, Berlin, 1989), p. 53.
[21] From the calculated vacancy density profile given in Ref. 5.
[22] G. F. Cerofolini, L. Meda, R. Balboni, F. Corni, S. Frabboni, G. Ottaviani, R. Tonini, M. Anderle, and R. Canteri, Phys. Rev. B **46**, 2061 (1992).
[23] G. D. Watkins and J. W. Corbett, Phys. Rev. **138**, A543 (1965).
[24] J. Mäkinen, C. Corbel, P. Hautojärvi, P. Moser, and F. Pierre, Phys. Rev. B **39**, 10 162 (1989).
[25] M. J. Puska, C. Corbel, and R. M. Nieminen, Phys. Rev. B **41**, 9980 (1990).
[26] S. Dannefaer, Phys. Status Solidi A **102**, 481 (1987).
[27] A. Dupasquier and L. Quartapelle, Appl. Phys. A **44**, 239 (1987).
[28] S. Valkealathi and R. M. Nieminen, Appl. Phys. A **35**, 51 (1984).
[29] R. S. Brusa, A. Dupasquier, E. Galvanetto, and A. Zecca, Appl. Phys. A **54**, 233 (1992).

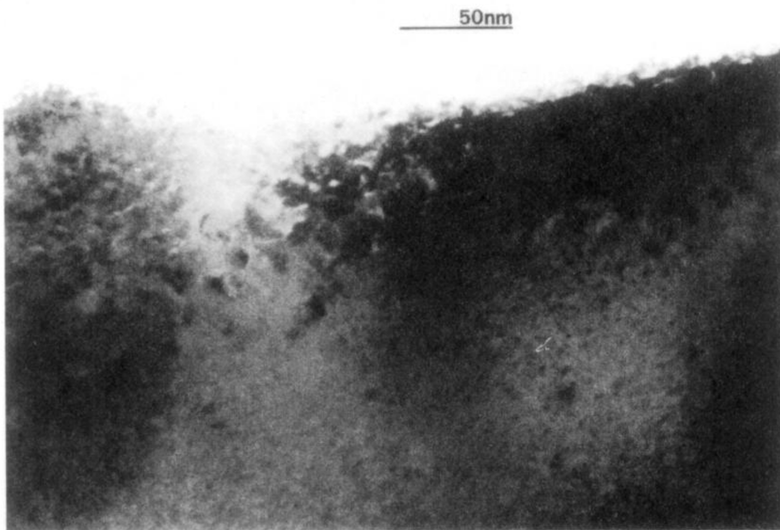

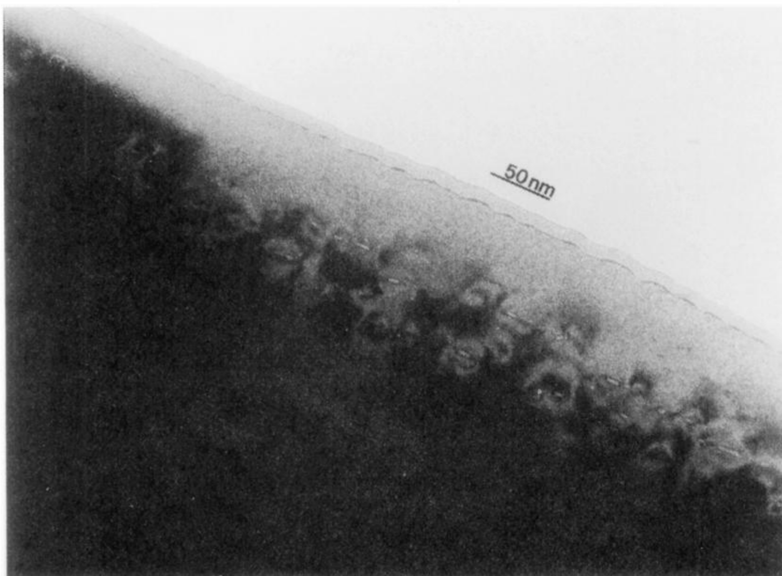

FIG. 6. TEM cross section of three RT(p) samples: (a) as-implanted; (b) annealed at 400 °C; (c) annealed at 600 °C.